Design and measurement of a piezoresistive triaxial accelerometer based on MEMS technology*

Du Chunhui(杜春晖)[1,2,†], He Changde(何常德)[1,2], Yu Jiaqi(于佳琪)[1], Ge Xiaoyang(葛晓洋)[1], Zhang Yongping(张永平)[2], and Zhang Wendong(张文栋)[1,2]

[1]Key Laboratory of Instrumentation Science & Dynamic Measurement, Ministry of Education, North University of China, Taiyuan 030051, China

[2]Key Laboratory of Science and Technology on Electronic Test & Measurement, North University of China, Taiyuan 030051, China

Abstract: With the springing up of the MEMS industry, research on accelerometers is focused on miniaturization, integration, high reliability, and high resolution, and shares extensive application prospects in military and civil fields. Comparing with the traditional single cantilever beam structure or "cantilever-mass" structure, the proposed structure of "8-beams/mass" with its varistor completely symmetric distribution in micro-silicon piezoresistive triaxial accelerometer in this paper has a higher axial sensitivity and smaller cross-axis sensitivity. Adopting ANSYS, the process of structural analysis and the manufacturing flow of sensing unit are showed. In dynamic testing conditions, it can be concluded that the axial sensitivity of x, y, and z are $S_x = 48$ μV/g, $S_y = 54$ μV/g and $S_z = 217$ μV/g respectively, and the nonlinearities are 0.4%, 0.6% and 0.4%.

Key words: cross-axis sensitivity; piezoresistive; symmetric distribution; triaxial accelerometer

DOI: 10.1088/1674-4926/33/10/104005 **EEACC:** 2570

1. Introduction

Accelerometers are commonly used in the fields of aerospace, biology, chemistry, medical analysis, automatic control, and vibration testing as inertial devices. Accelerometers based on MEMS technology are popular due to their small size, light weight, high sensitivity, strong antiradiation, mass-production, and other features[1]. Accelerometers are increasingly needed in automobile airbags, car navigation, consumer electronic products, the adjustment of elevator comfort degree, the detection of seismic waves, military inertial navigation, and penetration missile fuzes[2, 3]. There are many types of micromachined accelerometers, such as piezoresistive, piezoelectric, capacitive, and thermoelectric ones. Piezoresistive accelerometers gradually attract people's attention due to several advantages such as simple structure, high sensitivity, small nonlinearity, and low power dissipation[4].

The sensing unit of a piezoresistive micro-accelerometer consists of a movable mass: cantilevers overhanging between the mass and supporting rim. The number of cantilevers range from one root to eight. Usually, varistors are placed in the position bearing the maximum stress in the cantilever, and are fabricated by ion implantation. Thus varistors and resistance on the rim or external resistance constitute the Wheatstone bridge. The acceleration can be calculated by detecting the output voltage of the Wheatstone bridge. Therefore, only one or two of the four resistors are fabricated in the cantilever of the Wheatstone detection circuit. The disadvantages of such an approach are: first, as the half-bridge method is used in the Wheatstone bridge, the change of stress in the cantilever cannot be taken full use of. Due to this issue, the accelerometer cannot obtain maximum sensitivity[4]. Secondly, the fabrication of varistors in the cantilever will inevitably introduce residual stress, which may lead to drift. The drift caused by asymmetry of the four resistors in the Wheatstone bridge will lead to an increase of zero drift. Finally, the anisomerous distribution of varistors in cantilever will lead to an uneven distribution of stress on the cantilever, which may cause the increase of coupling between the axis.

Based on the above analysis, a kind of single-chip triaxial accelerometer with a highly symmetric structure is proposed in this paper. The accelerometer avoids the installation errors caused by installing three independent single-axis accelerometers in three mutually perpendicular directions[5]. Meanwhile, is has high sensitivity, weak coupling and low non-linearity. The design, fabrication and test process are as follows.

2. Design and simulation

2.1. Device structure designed

Figure 1(a) shows the structure of a piezoresistive triaxial accelerometer. The device has a double-layer package structure, which is fabricated by anodic bonding techniques. The anodic bonding technology plays a role of overload protection. The varistor distribution of the piezoresistive triaxial accelerometer is shown in Fig. 1(b). 16 varistors are distributed symmetrically in 8 cantilevers. When acceleration is applied in

* Project supported by the International Science & Technology Cooperation Program of China (No. 61011140351), the National High Technology Research and Development Program of China (No. 2011AA040404), and the National Natural Science Foundation of China (No. 51075375).

† Corresponding author. Email: duchunhui319@163.com

Received 27 March 2012, revised manuscript received 17 May 2012

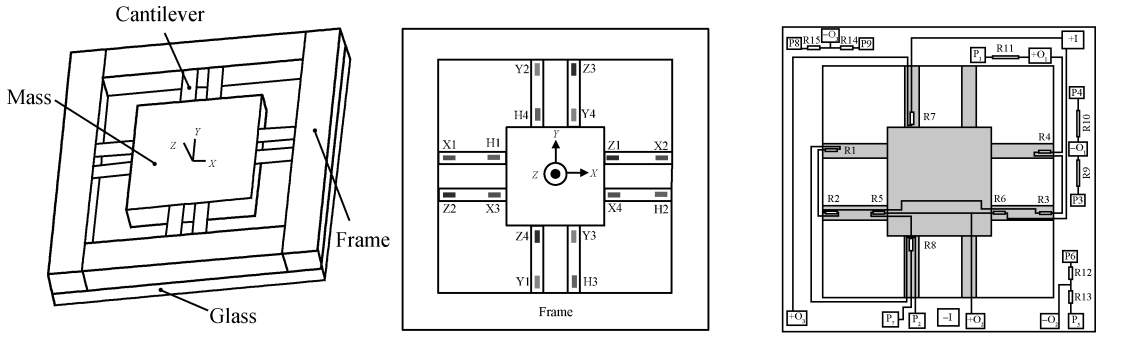

(a) Whole structure (b) Varistor distribution (c) Varistor distribution of the sense structure

Fig. 1. Micro-silicon piezoresistive triaxial accelerometer.

Table 1. Output sensitivity and cross-axis sensitivity of the sense structure shown in Fig. 1(c).

Parameter	x	y	z
Output sensitivity/ cross-axis sensitivity of x	0.06 μV/g	28.9%	8.2%
Output sensitivity/ cross-axis sensitivity of y	32.5%	0.052 μV/g	7.6%
Output sensitivity/ cross-axis sensitivity of z	52.7%	42%	0.82 μV/g

a certain direction, each cantilever bears the pressure and tension equally. A detection circuit will have an output voltage as four varistors of the Wheatstone bridge bear cross-stress in the major axis. While in other directions, there is no output voltage due to stress offsetting. Acceleration can be calculated according to the output voltage. Characteristics of this accelerometer include: (1) the excellent symmetry structure both improves the axial sensitivity and reduces the cross-axis sensitivity; (2) the symmetrical distribution of varistors can effectively inhibit drift caused by residual stress; (3) the thickness of the SOI is fully used to form large mass then to improve the SNR. Compared with other domestic piezoresistive triaxial accelerometers, this accelerometer has higher sensitivity and lower cross-axis sensitivity. The varistor distribution of another triaxial accelerometer developed by the North University of China is shown in Fig. 1(c). Table 1 shows the output sensitivity and the cross-axis sensitivity of this structure.

2.2. Device parameters design

2.2.1. Mass

In order to increase the axial sensitivity and SNR, the mass should be as large as possible in the range of elastic stress of Si[6]. The mass of the accelerometer is determined for 3 × 3 mm^2.

Thickness of the SOI has been etched 10 μm then formed the mass whose thickness is about 420 μm. The mass is fabricated by using an ICP etching process.

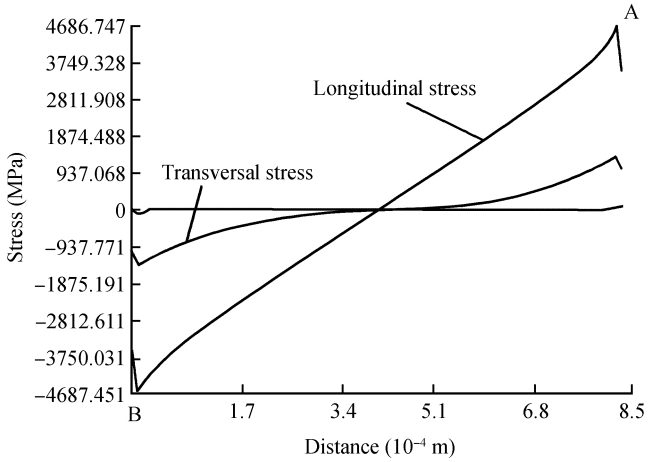

Fig. 2. Stress distribution on the cantilever.

2.2.2. Cantilevers

The eight cantilevers are symmetrically distributed around the mass. The length of the cantilever is proportional to sensitivity, and inversely proportional to resonant frequency. The width and thickness of the cantilever are inversely proportional to sensitivity, but are proportional to resonant frequency. In consideration of various factors and the process technology limits of 55th Institute of China Electronics Technology Group Corporation, eventually the size of the cantilevers is determined to be 800 × 300 × 20 μm^3.

2.2.3. Varistors

The sensitivity is affected by the location of varistors to a great extent. P-type varistors have larger resistance change rate than the N-type. So P-type varistors are placed where the stress changes most. In order to improve the linearity of the sensor's output voltage, varistors should be put in the linear region. The distribution of varistors should be near the center, while deviating from A and B, as Figure 2 shows. The change rate of the varistor is:

$$\frac{\Delta R}{R} = \pi_{\mathrm{l}}\sigma_{\mathrm{l}} + \pi_{\mathrm{t}}\sigma_{\mathrm{t}} + \pi_{\mathrm{s}}\sigma_{\mathrm{s}}, \tag{1}$$

σ_{l} is transverse stress, σ_{t} is longitudinal stress, σ_{s} is vertical stress, σ_{s} is generally ignored as it is far smaller than σ_{l} and σ_{t};

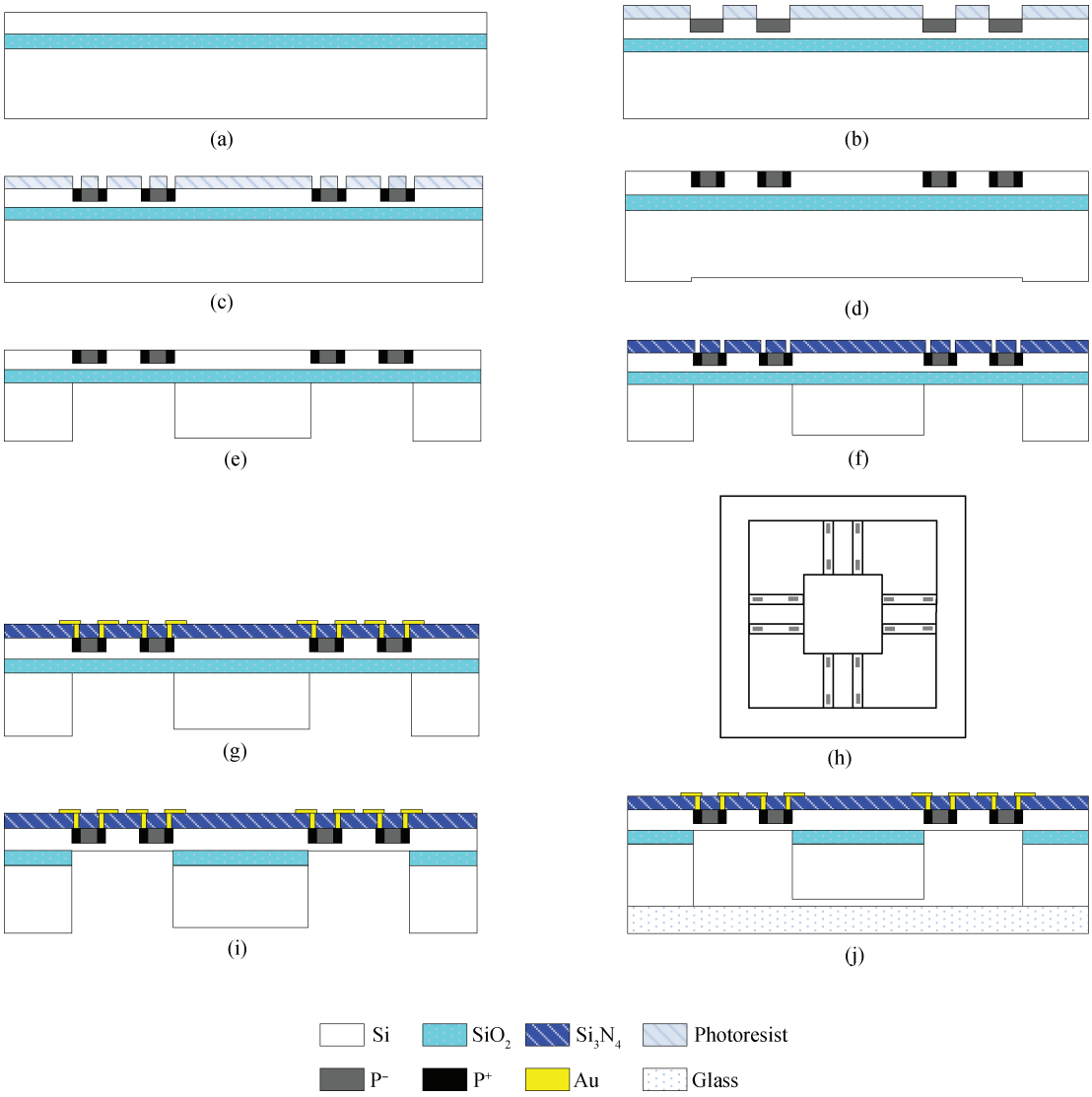

Fig. 3. Process flow.

π_l, π_t, π_s are piezoresistance coefficients, respectively, corresponding to σ_l, σ_t, σ_s. So Equation (1) is simplified:

$$\frac{\Delta R}{R} = \pi_l\sigma_l + \pi_t\sigma_t = (71.8\sigma_l - 66.3\sigma_t) \times 10^{-11}. \quad (2)$$

It is concluded from the Wheatstone bridge that the output voltage of x, y, and z is:

$$\begin{aligned} V_{\mathrm{OUTX}} &= \left(\frac{R_{\mathrm{X3}} + \Delta R_{\mathrm{X3}}}{R_{\mathrm{X1}} + \Delta R_{\mathrm{X1}} + R_{\mathrm{X3}} + \Delta R_{\mathrm{X3}}} - \frac{R_{\mathrm{X4}} + \Delta R_{\mathrm{X4}}}{R_{\mathrm{X2}} + \Delta R_{\mathrm{X2}} + R_{\mathrm{X4}} + \Delta R_{\mathrm{X4}}}\right) V_{\mathrm{CC}} \\ &= \left(\frac{1 + \dfrac{\Delta R_{\mathrm{X3}}}{R}}{2 + \dfrac{\Delta R_{\mathrm{X1}}}{R} + \dfrac{\Delta R_{\mathrm{X3}}}{R}} - \frac{1 + \dfrac{\Delta R_{\mathrm{X4}}}{R}}{2 + \dfrac{\Delta R_{\mathrm{X2}}}{R} + \dfrac{\Delta R_{\mathrm{X4}}}{R}}\right) \times V_{\mathrm{CC}}, \end{aligned} \quad (3)$$

$$\begin{aligned} V_{\mathrm{OUTY}} &= \left(\frac{R_{\mathrm{Y3}} + \Delta R_{\mathrm{Y3}}}{R_{\mathrm{Y1}} + \Delta R_{\mathrm{Y1}} + R_{\mathrm{Y3}} + \Delta R_{\mathrm{Y3}}} - \frac{R_{\mathrm{Y4}} + \Delta R_{\mathrm{Y4}}}{R_{\mathrm{Y2}} + \Delta R_{\mathrm{Y2}} + R_{\mathrm{Y4}} + \Delta R_{\mathrm{Y4}}}\right) V_{\mathrm{CC}} \\ &= \left(\frac{1 + \dfrac{\Delta R_{\mathrm{Y3}}}{R}}{2 + \dfrac{\Delta R_{\mathrm{Y1}}}{R} + \dfrac{\Delta R_{\mathrm{Y3}}}{R}} - \frac{1 + \dfrac{\Delta R_{\mathrm{Y4}}}{R}}{2 + \dfrac{\Delta R_{\mathrm{Y2}}}{R} + \dfrac{\Delta R_{\mathrm{Y4}}}{R}}\right) \times V_{\mathrm{CC}}, \end{aligned} \quad (4)$$

$$\begin{aligned} V_{\mathrm{OUTZ}} = [&(R_{\mathrm{Z3}} + \Delta R_{\mathrm{Z3}} + R_{\mathrm{H3}} + \Delta R_{\mathrm{H3}}) \\ &\times (R_{\mathrm{Z1}} + \Delta R_{\mathrm{Z1}} + R_{\mathrm{H1}} + \Delta R_{\mathrm{H1}} + R_{\mathrm{Z3}} + \Delta R_{\mathrm{Z3}} \\ &+ R_{\mathrm{H3}} + \Delta R_{\mathrm{H3}})^{-1} \\ &- (R_{\mathrm{Z4}} + \Delta R_{\mathrm{Z4}} + R_{\mathrm{H4}} + \Delta R_{\mathrm{H4}}) \\ &\times (R_{\mathrm{Z2}} + \Delta R_{\mathrm{Z2}} + R_{\mathrm{H2}} + \Delta R_{\mathrm{H2}} + R_{\mathrm{Z4}} + \Delta R_{\mathrm{Z4}} \\ &+ R_{\mathrm{H4}} + \Delta R_{\mathrm{H4}})^{-1}] V_{\mathrm{CC}} \end{aligned}$$

$$= \left(\frac{2 + \frac{\Delta R_{Z3}}{R} + \frac{\Delta R_{H3}}{R}}{4 + \frac{\Delta R_{Z1}}{R} + \frac{\Delta R_{H1}}{R} + \frac{\Delta R_{Z3}}{R} + \frac{\Delta R_{H3}}{R}} - \frac{2 + \frac{\Delta R_{Z4}}{R} + \frac{\Delta R_{H4}}{R}}{4 + \frac{\Delta R_{Z2}}{R} + \frac{\Delta R_{H2}}{R} + \frac{\Delta R_{Z4}}{R} + \frac{\Delta R_{H4}}{R}} \right) V_{CC}. \quad (5)$$

If the acceleration is only loaded in the x direction, the absolute value of the $\frac{\Delta R_{X1}}{R}$, $\frac{\Delta R_{X2}}{R}$, $\frac{\Delta R_{X3}}{R}$, $\frac{\Delta R_{X4}}{R}$ is almost equality, whereas, the sign of $\frac{\Delta R_{X1}}{R}$, $\frac{\Delta R_{X4}}{R}$ and $\frac{\Delta R_{X2}}{R}$, $\frac{\Delta R_{X3}}{R}$ is reverse; $\frac{\Delta R_{Y1}}{R}$, $\frac{\Delta R_{Y2}}{R}$, $\frac{\Delta R_{Y3}}{R}$, $\frac{\Delta R_{Y4}}{R}$ have the same absolute value and sign. $\frac{\Delta R_{Z1}}{R}$, $\frac{\Delta R_{Z2}}{R}$, $\frac{\Delta R_{H1}}{R}$, $\frac{\Delta R_{H2}}{R}$ have the same absolute value and sign. $\frac{\Delta R_{Z3}}{R}$, $\frac{\Delta R_{Z4}}{R}$, $\frac{\Delta R_{H3}}{R}$, $\frac{\Delta R_{H4}}{R}$ have the same absolute value and sign.

By the analysis: $V_{OUTX} = \frac{\frac{\Delta R_{X3}}{R} - \frac{\Delta R_{X4}}{R}}{2} V_{CC}$; $V_{OUTY} \approx 0$; $V_{OUTZ} \approx 0$.

In the same way, if the acceleration is only loaded in the y direction: $V_{OUTX} \approx 0$; $V_{OUTY} = \frac{\frac{\Delta R_{Y3}}{R} - \frac{\Delta R_{Y4}}{R}}{2} V_{CC}$; $V_{OUTZ} \approx 0$.

If the acceleration is only loaded in the z direction: $V_{OUTX} \approx 0$; $V_{OUTY} \approx 0$; $V_{OUTZ} = \frac{\frac{\Delta R_{Z3}}{R} + \frac{\Delta R_{H3}}{R} - \frac{\Delta R_{Z4}}{R} - \frac{\Delta R_{H4}}{R}}{4} V_{CC}$.

3. Fabrication process

The ϕ100 mm N type (100) SOI substrate of the accelerometer was chosen as the starting material. The thickness of the active layer is 20 $\pm$ 1 μm, and resistivity is 2–4 Ω·cm; the thickness of the box layer is 0.5 $\pm$ 0.1 μm; the thickness of the handle wafer is 410 $\pm$ 10 μm, and resistivity is 2–4 Ω·cm. The fabrication process of the accelerometer is shown in Fig. 3. (a) the starting material: ϕ100 mm N type (100) SOI substrate; (b) boron doping: boron was diffused to form arrestors; (c) heavy boron doping: heavy p+-doping silicon was formed on the two sides of the arrestors; (d) slight etching on the backside: a 10 μm deep platform was etched by ICP technology to form the activity space; (e) formation of mass: the back of the substrate was etched by ICP technology; (f) deposition of Si_3N_4 by PECVD: Si_3N_4 was deposited by PECVD on top of the active layer. An electrode contact hole was etched on Si_3N_4; (g) deposition of metal by thermal evaporator: first Cr, 500 Å, then Au, 1000 Å, unnecessary metal was removed to produce metal wire. (h) ICP etching: cantilevers were released on the positive side by ICP technology; (i) RIE etching: SiO_2 was etched on the back of the cantilevers; (j) bonding glass to substrate: glass was bonded to substrate by using anodic bonding technology.

The dicing size of the fabricated accelerometer is 6 $\times$ 6 mm^2. Figure 4(a) shows the whole structure of the fabricated triaxial accelerometer. Figure 4(b) shows a local amplification image of the cantilever. Figure 4(c) shows a packaged accelerometer.

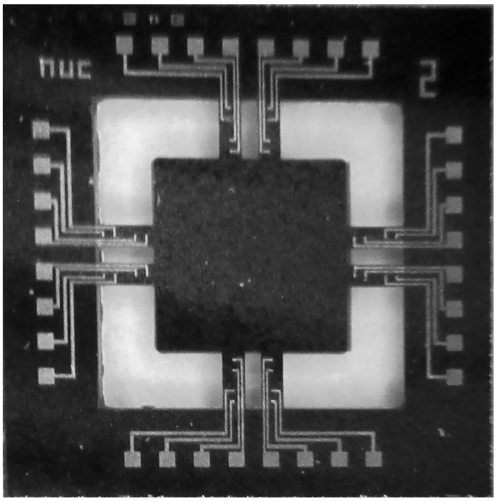

(a)

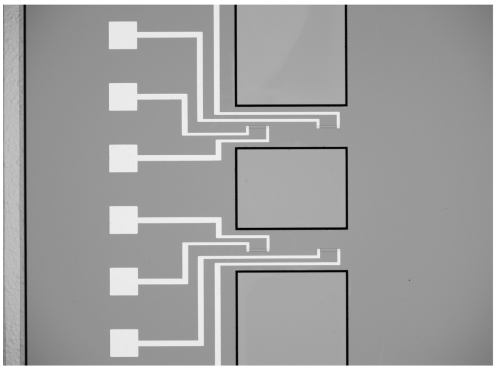

(b)

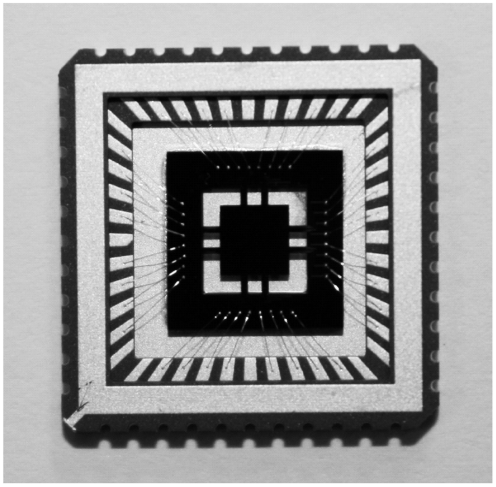

(c)

Fig. 4. Photos of completed chip.

4. Test

It is relatively difficult to test the accelerometer, especially the low-range accelerometer. Measurement errors are easily introduced due to the high sensitivity of the installation process. In addition, large errors will be introduced by vibration of the test platform. Precision centrifuge provides a reliable method to test low-g accelerometers, because of its stable rotation and accurate output. The following figures are test results by precision centrifuging.

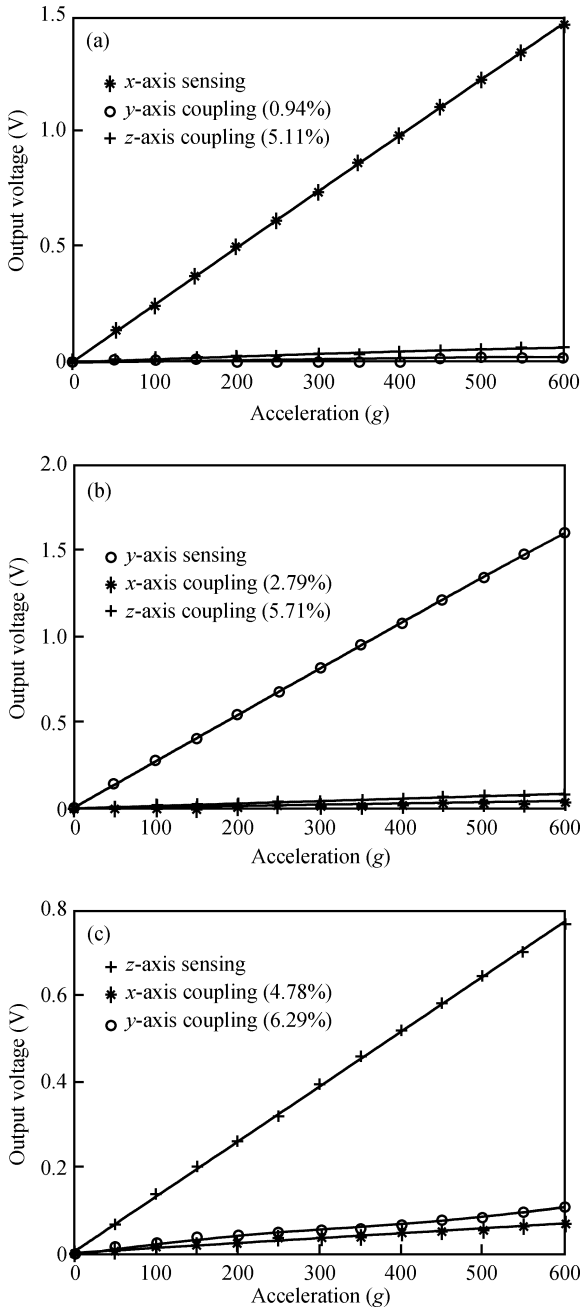

Fig. 5. Testing platform of the precision centrifuge and output characteristics of the accelerometer. (a) x-component. (b) y-component. (c) z-component.

The accelerometer is installed in the rotating platform of the precision centrifuge, making sure that the measured direction points to the axis of the precision centrifuge. The rotating platform of the precision centrifuge is balanced by a same quality device with an accelerometer.

Test conditions: signals in x-axis and y-axis are magnified 50 times, while 10 times in z-axis, the rotation radius of accelerometer is 220 mm, and the tolerance of the precision centrifuge is $\leqslant 1\%$.

Figures 5(a)–5(c) show the curves of the accelerometer output. Load acceleration ranging from 0 to 600 g is applied on the accelerometer, while the load interval is 50 g. The output voltage is obtained by using a high precision multimeter. The output curves are calculated by their averages. Results are: the sensitivity of x-axis is $S_x = 48$ μV/g, nonlinearity is 0.4% and coupling to y-axis and z-axis are $S_y/S_x = 0.94\%$ and $S_z/S_x = 5.11\%$; the sensitivity of the y-axis is $S_y = 54$ μV/g, nonlinearity is 0.6% and coupling to x-axis and z-axis are $S_x/S_y = 2.79\%$, $S_z/S_y = 5.71\%$; the sensitivity of the z-axis is $S_z = 217$ μV/g, nonlinearity is 0.4% and coupling to x-axis and y-axis are $S_x/S_z = 4.78\%$, $S_y/S_z = 6.29\%$.

5. Conclusion

A monolithically integrated triaxial MEMS accelerometer has been designed, fabricated and tested in this paper. It has many advantages, such as high sensitivity, low nonlinearity and so on. The test results have proved that the design concept is correct and the technological process is feasible. The accelerometer will be applied in civil products if the technological process and package are optimized to get better consistency and smaller size. As a single-axis accelerometer, the sensitivity and linearity of z-axis are better than similar domestic products.

References

[1] Zhang Jianbi. MEMS-based micro-silicon piezoresistive accelerometer design. Electron Sci Technol, 2009, 22(10): 40
[2] Yazdi N, Ayazi F, Najafi K. Micromachined inertial sensors. Proc IEEE, 1998, 86(8): 1640
[3] Najafi K, Chac J, Kulah H, et al. Micromachined silicon accelerometers and gyroscopes. IEEE/RSJ International Conference on Intelligent Robots and Systems, 2003, 3: 2353
[4] Wu Rui, Wen Tingdun. Silicon micro-acceleration sensor technologies. Instrument Technique and Sensor, 2007, (3): 8
[5] Dong Peitao, Li Xinxin, Zhang Kun, et al. Design, fabrication and characterization of a high-performance monolithic triaxial piezoresistive high-g accelerometer. Chinese Journal of Semiconductors, 2007, 28(9): 1482
[6] Wang Yucai, Jiao Jiwei, Duan Fei, et al. Design and fabrication of an accelerometer with novel "8-beams/mass" structure. Chinese Journal of Semiconductors, 2007, 28(5): 783
[7] Takao H, Matsumoto Y, Ishida M. A monolithically integrated three axial accelerometer using stress sensitive CMOS differential amplifiers. International Conference on Solid-State Sensor and Actuators, 1997: 1173
[8] Takao H, Fukumoto H, Ishida M. Fabrication of a three-axis accelerometer integrated with commercial 0.8 μm-CMOS circuits. Proc IEEE 13th Annu Int Conf Micro Electro Mechanical Systems, 2000: 781
[9] Takao H, Fukumoto H, Ishida M. A CMOS integrated three-axis accelerometer fabricated with commercial submicrometer CMOS technology and bulk-micromachining. IEEE Trans Electron Devices, 2001, 48(9): 1961